Dinuclear Acetylide-bridged Ruthenium(II) Complexes with Rigid Non-aromatic Spacers Supplementary Information

Surabhi Naik, Synøve Ø. Scottwell, Hsiu L. Li, Chanel F. Leong, Deanna M. D'Alessandro, Leslie D. Field*.

Contents

S1 Compound numbers and labelling conventions

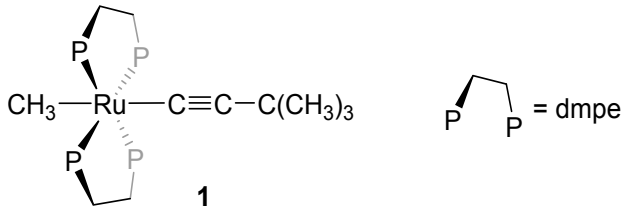

1

[*trans*-Ru(dmpe)$_2$(C≡C^{t}Bu)(CH$_3$)] (**1**)

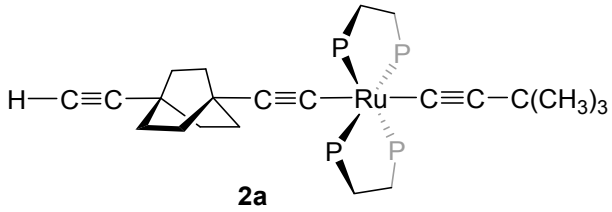

2a

[*trans*-Ru(dmpe)$_2$(C≡C^{t}Bu)(C≡C-C$_8$H$_{12}$-C≡CH)] (**2a**)

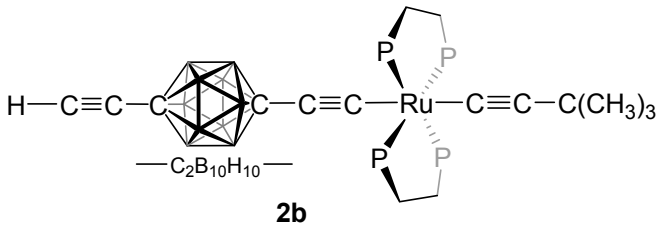

2b

[*trans*-Ru(dmpe)$_2$(C≡C^{t}Bu)(C≡C-*p*-C$_2$B$_{10}$H$_{10}$-C≡CH)] **(2b)**

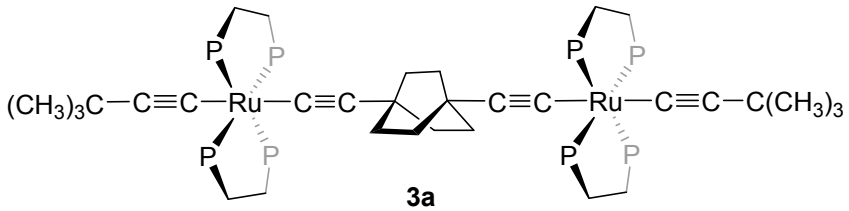

3a

[*trans,trans*-{Ru(dmpe)$_2$(C≡C^{t}Bu)}$_2$(*μ*-C≡C-C$_8$H$_{12}$-C≡C)] (**3a**)

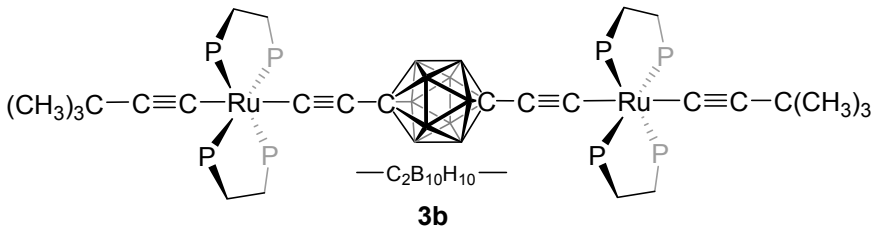

3b

[*trans,trans*-{Ru(dmpe)$_2$(C≡C^{t}Bu)}$_2$(*μ*-C≡C-*p*-C$_2$B$_{10}$H$_{10}$-C≡C)] (**3b**)

S2 NMR Data

S2.1 ^{1}H, $^{1}H\{^{31}P\}$, $^{31}P\{^{1}H\}$, and $^{13}C\{^{1}H\}$ NMR spectra of [trans-Ru(dmpe)$_2$(C≡C^{t}Bu)(C≡C-C$_8$H$_{12}$-C≡CH)] (2a)

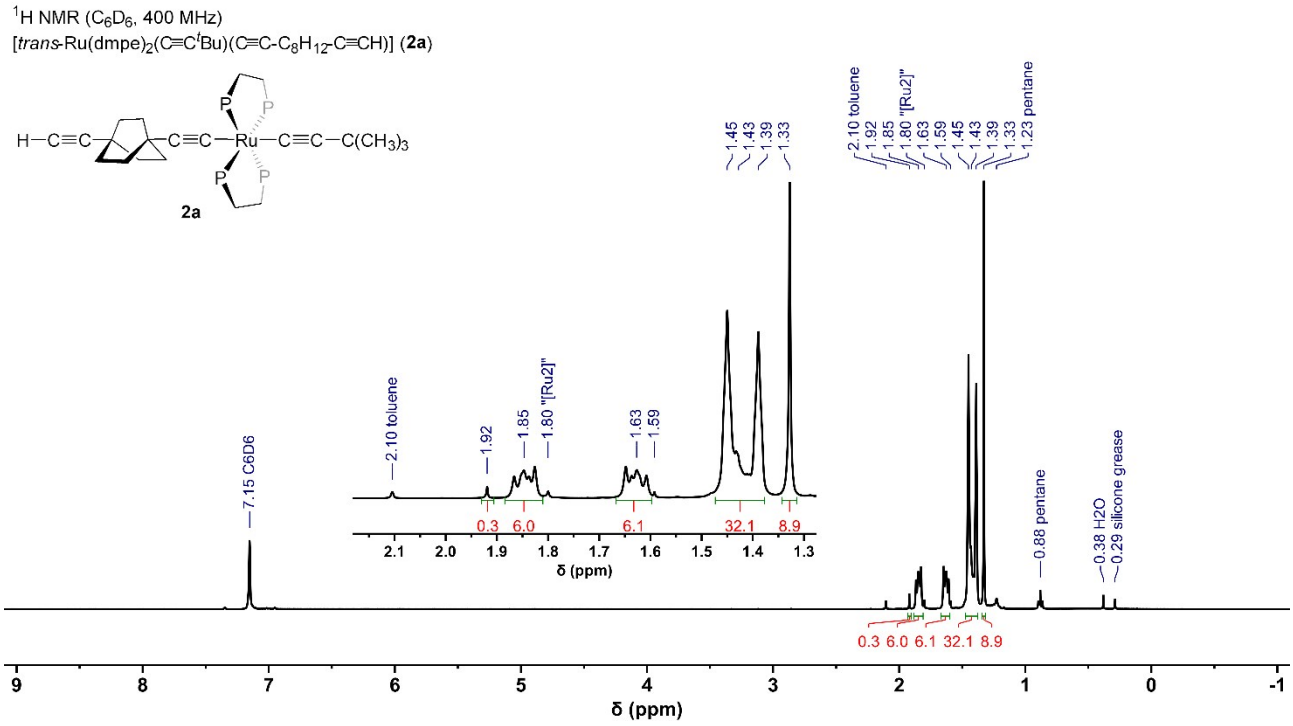

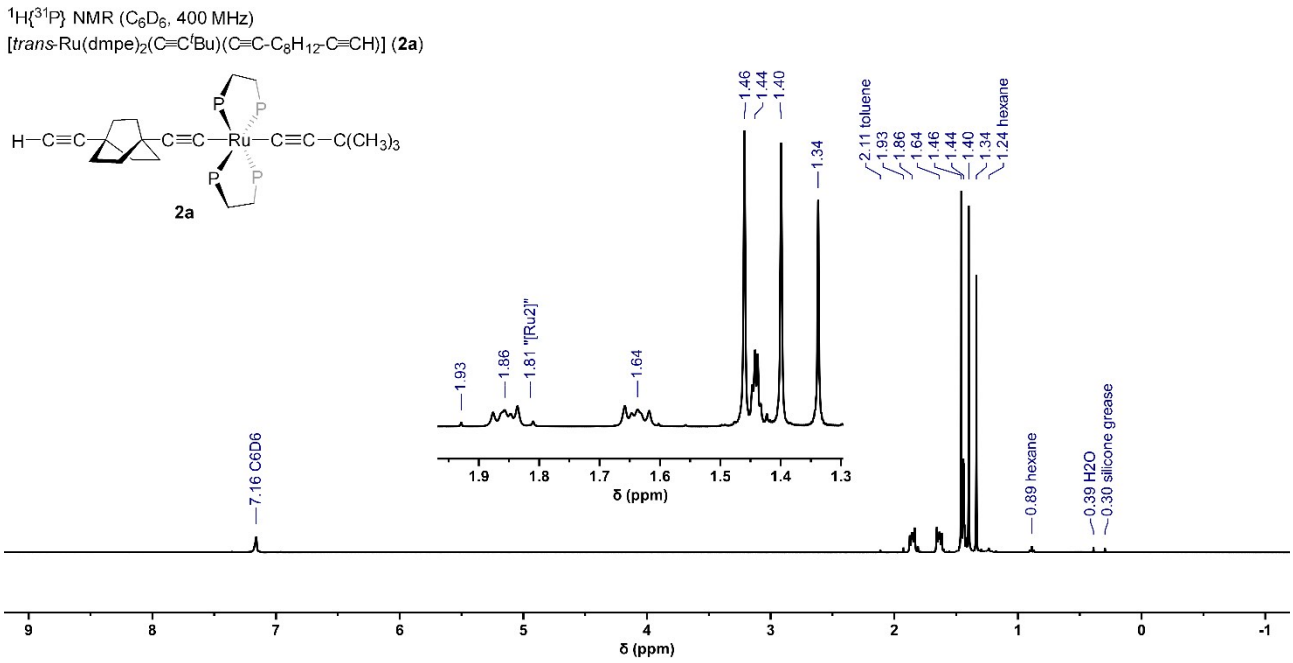

$^{31}P\{^{1}H\}$ NMR (C_6D_6, 162 MHz)
[*trans*-Ru(dmpe)$_2$(C≡C^{t}Bu)(C≡C-C$_8$H$_{12}$-C≡CH)] (**2a**)

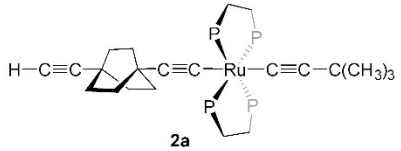

2a

$^{13}C\{^{1}H\}$ NMR (C_6D_6, 101 MHz)
[*trans*-Ru(dmpe)$_2$(C≡C^{t}Bu)(C≡C-C$_8$H$_{12}$-C≡CH)] (**2a**)

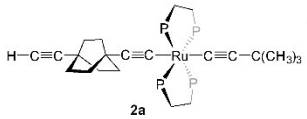

2a

S2.1.1 Assignment of acetylenic ^{13}C NMR resonances of [trans-Ru(dmpe)$_2$(C≡C^{t}Bu)(C≡C-C$_8$H$_{12}$-C≡CH)] (2a)

The ^1H and ^{13}C NMR resonances for complex **2a** were assigned using a range of 2D NMR experiments. Resonances arising from alkyl groups on the complex (environments i/j, k, o, labelling scheme in Figure S1) were identified in a straightforward manner using multiplicity-edited ^1H-^{13}C heteronuclear single quantum coherence (HSQC) spectroscopy. The terminal acetylenic carbon $\mathbf{C_a}$ was likewise identified by a ^1H-^{13}C HSQC correlation to the acetylenic proton resonance.

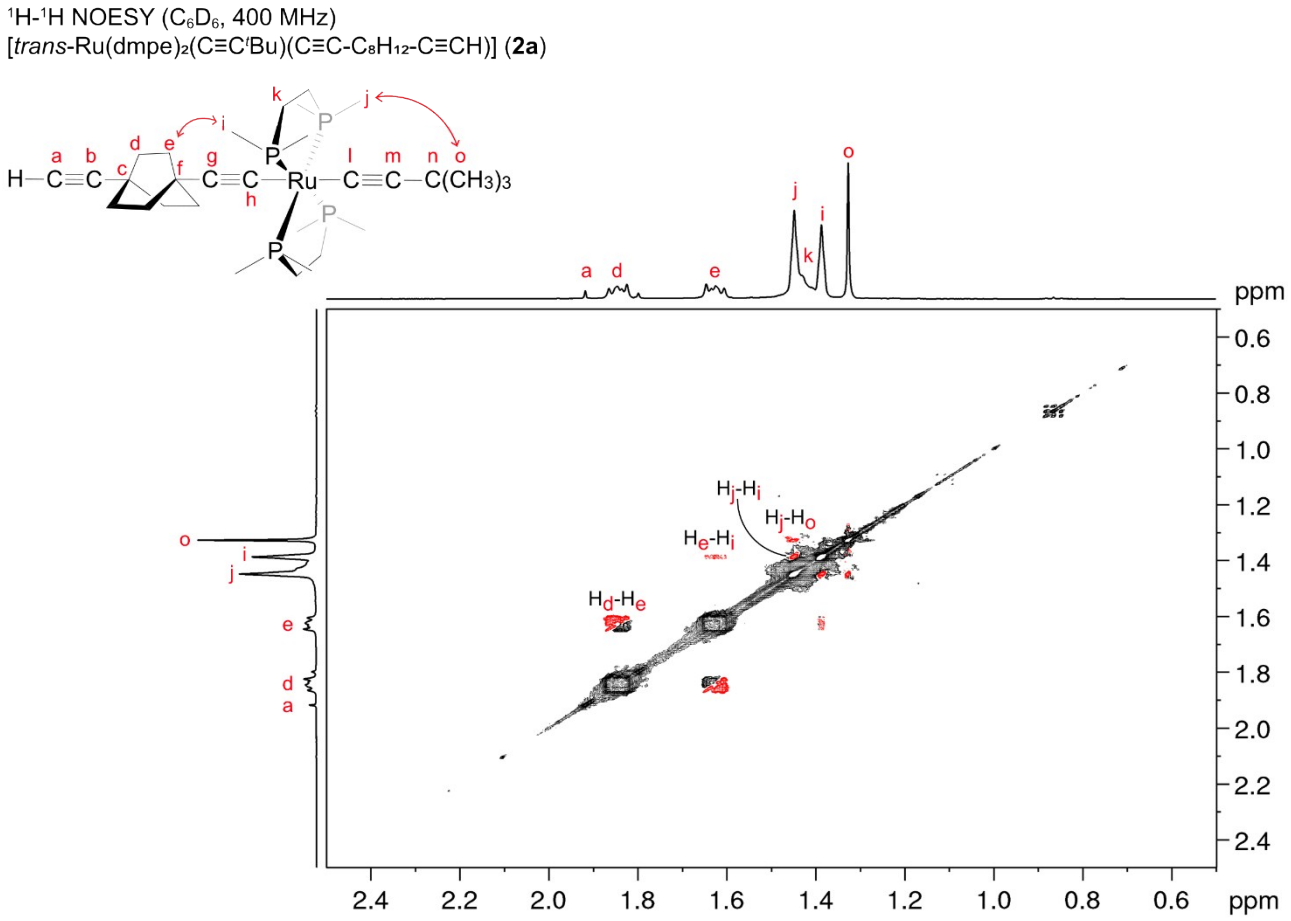

*Figure S1. Zoomed ^1H-^1H NOESY spectrum of complex **2a**; NB: indicated labelling of nuclear environments does not correspond to labelling scheme of acetylenic carbons in manuscript.*

The ^1H-^1H NOESY (nuclear Overhauser effect spectroscopy) spectrum of complex **2a** (Figure S1) enabled identification of the two inequivalent methyl resonances ($\mathbf{H_i}$ and $\mathbf{H_j}$) bound to the phosphorus atoms. Each methyl group exhibited separate NOE interactions with either the protons on the capping *tert*-butyl group ($\mathbf{H_o}$) or the one of the bicyclooctyl bridge proton environments ($\mathbf{H_e}$). This then enabled the assignment of the two bridge proton resonances, $\mathbf{H_d}$ and $\mathbf{H_e}$.

Acetylenic carbons $\mathbf{C_b}$, $\mathbf{C_g}$ and $\mathbf{C_m}$ were easily distinguished by strong correlations in ^1H-^{13}C HMBC spectrum (Figure S2) to $\mathbf{H_d}$, $\mathbf{H_e}$ and $\mathbf{H_o}$, respectively. Pentet resonances $\mathbf{C_h}$ and $\mathbf{C_l}$ were identified by

their 15 Hz coupling to 4 equivalent phosphorus atoms, and were differentiated by a weak correlation between $\mathbf{C_l}$ and $\mathbf{H_o}$ in ^{1}H-^{13}C HMBC spectrum. Carbons $\mathbf{C_h}$ and $\mathbf{C_l}$ also displayed HMBC correlations to either $\mathbf{H_i}$ and $\mathbf{H_j}$ on either side of the plane formed by equatorial P atoms.

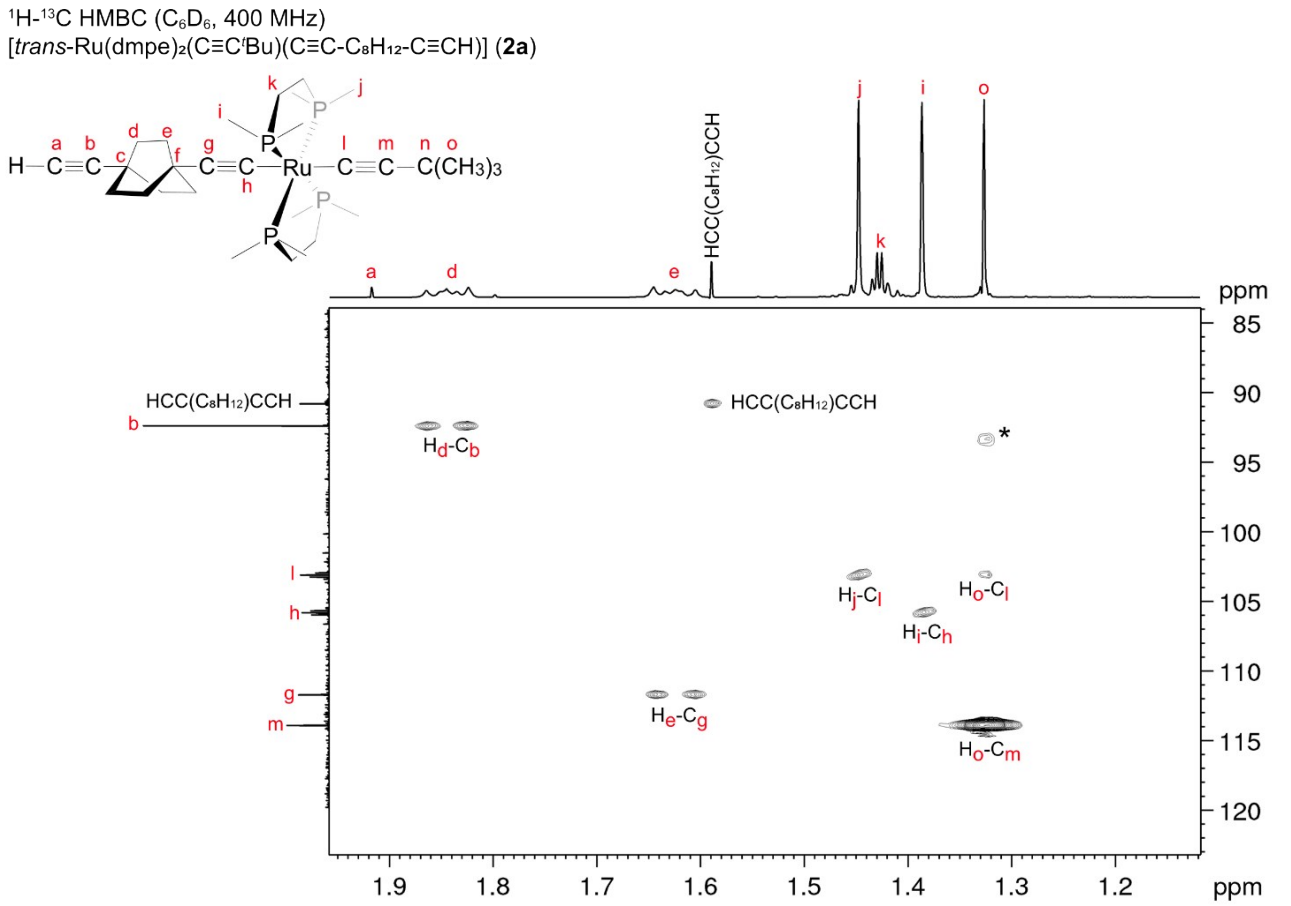

*Figure S2. Zoomed ^{1}H-^{13}C HMBC spectrum of complex **2a** showing relevant cross-peaks; NB: indicated labelling of nuclear environments does not correspond to labelling scheme of acetylenic carbons in manuscript.*

** Cross-peak arising from unidentified impurity.*

S2.2 ^{1}H, $^{1}H\{^{31}P\}$, $^{31}P\{^{1}H\}$, $^{11}B\{^{1}H\}$, and $^{13}C\{^{1}H\}$ NMR spectra of [trans-Ru(dmpe)$_2$(C≡C^{t}Bu)(C≡C-p-C$_2$B$_{10}$H$_{10}$-C≡CH)] (2b)

^{1}H NMR (C_6D_6, 400 MHz)
[*trans*-Ru(dmpe)$_2$(C≡C^{t}Bu)(C≡C-*p*-C$_2$B$_{10}$H$_{10}$-C≡CH)] (**2b**)

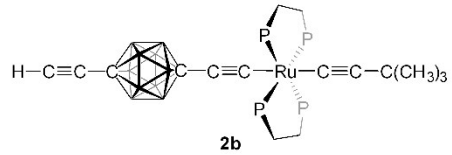

2b

$^{1}H\{^{31}P\}$ NMR (C_6D_6, 400 MHz)
[*trans*-Ru(dmpe)$_2$(C≡C^{t}Bu)(C≡C-*p*-C$_2$B$_{10}$H$_{10}$-C≡CH)] (**2b**)

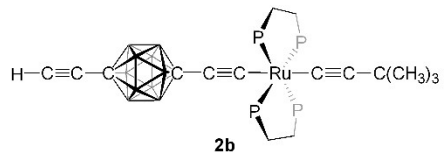

2b

$^{31}P\{^{1}H\}$ NMR (C_6D_6, 162 MHz)
[*trans*-Ru(dmpe)$_2$(C≡C^{t}Bu)(C≡C-*p*-$C_2B_{10}H_{10}$-C≡CH)] (**2b**)

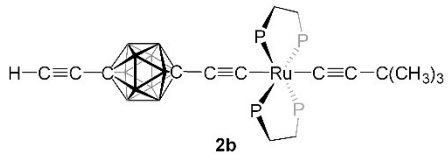

2b

$^{11}B\{^{1}H\}$ NMR (C_6D_6, 193 MHz)
[*trans*-Ru(dmpe)$_2$(C≡C^{t}Bu)(C≡C-*p*-$C_2B_{10}H_{10}$-C≡CH)] (**2b**)

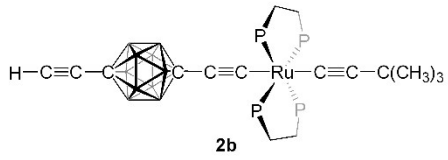

2b

$^{13}C\{^{1}H\}$ NMR (C_6D_6, 151 MHz)
[*trans*-Ru(dmpe)$_2$(C≡C^{t}Bu)(C≡C-*p*-$C_2B_{10}H_{10}$-C≡CH)] (**2b**)

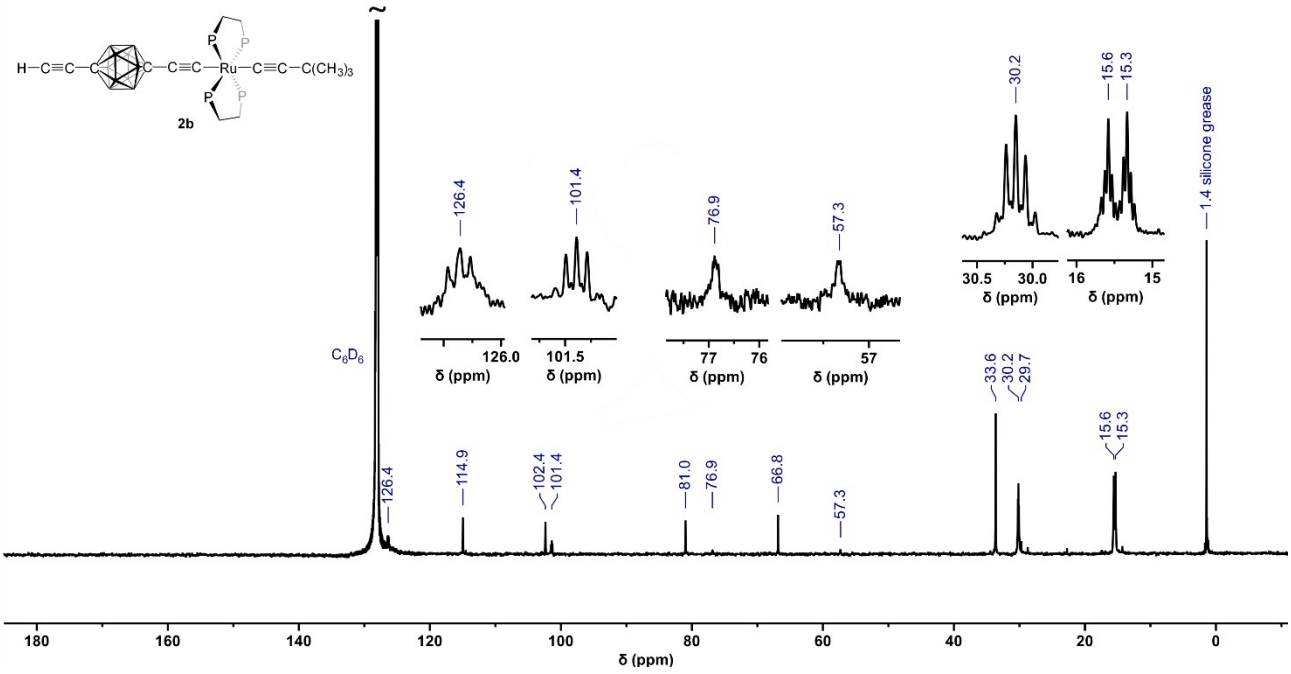

S2.2.1 Assignment of acetylenic ^{13}C NMR resonances of [trans-Ru(dmpe)$_2$(C≡C^{t}Bu)(C≡C-p-C$_2$B$_{10}$H$_{10}$-C≡CH)] (2b)

The ^{1}H and ^{13}C NMR resonances for complex **2b** were assigned, as with complex **2a** (see **S2.1.1**), using a range of 2D NMR experiments. The broadness of proton resonances arising from the *p*-carborane bridge (**H$_d$** and **H$_e$**, labelling scheme in Figure S3) prevented the detection of cross-peaks in the ^{1}H-^{13}C HMBC spectra of complex **2b** that would have allowed direct identification of carbons **C$_b$** or **C$_g$**; these carbon resonances have been tentatively assigned based on corresponding chemical shift values with analogous ^{13}C environments in complex **2a.**

Acetylenic carbon resonance **C$_m$** was identified by a strong correlation in ^{1}H-^{13}C HMBC spectrum to **H$_o$**. Pentet resonances **C$_h$** and **C$_l$** were, as with complex **2a**, identified by their 15-16 Hz coupling to 4 equivalent phosphorus atoms. These were differentiated by HMBC correlations to **H$_i$** and **H$_j$**, respectively, and assigned based on both analogous correlations in the ^{1}H-^{13}C HMBC spectrum of complex **2a**, as well as chemical shift values for NMR resonances arising from analogous ^{1}H and ^{13}C environments in complex **2a**.

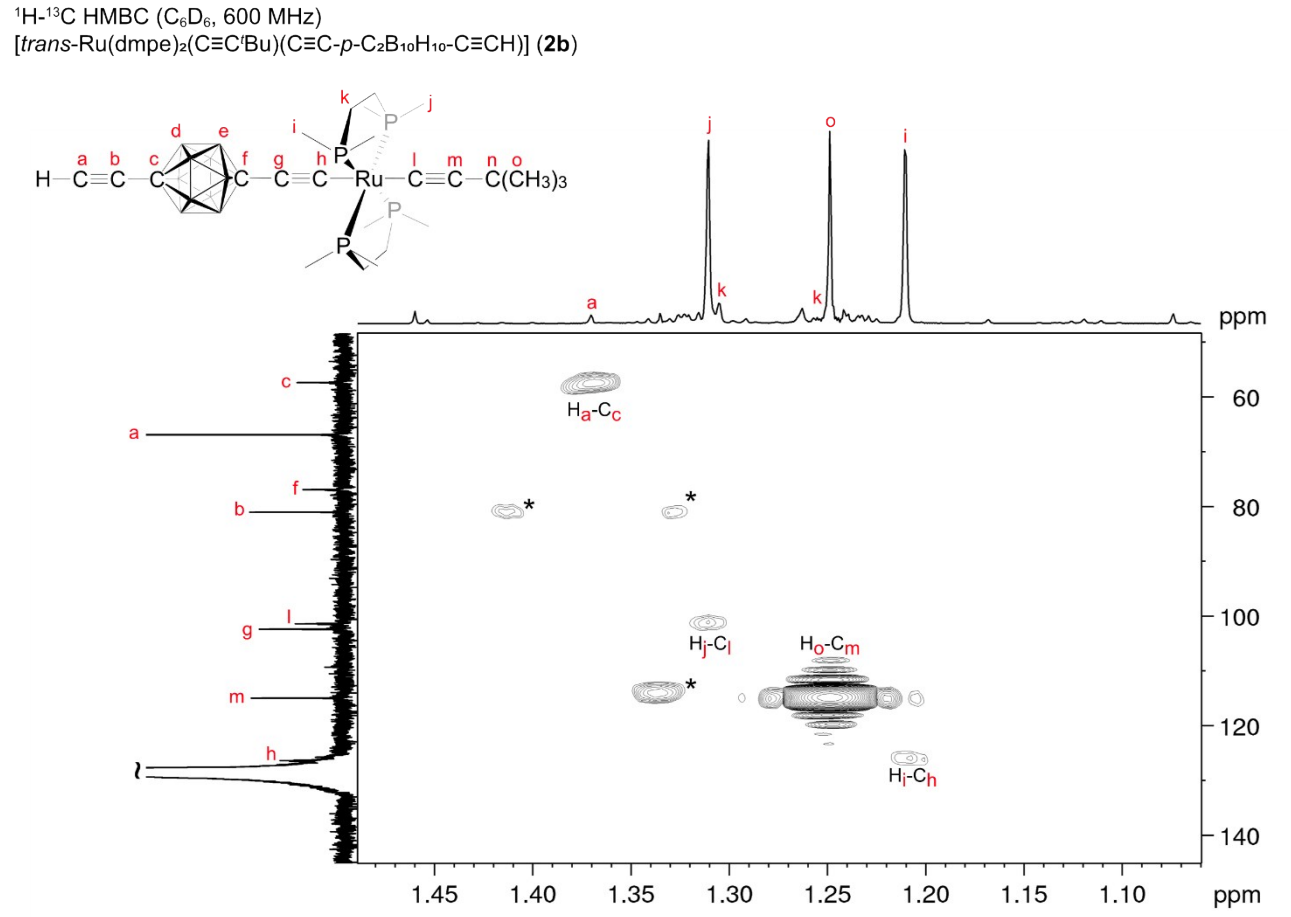

*Figure S3. Zoomed ^{1}H-^{13}C HMBC spectrum of complex **2b** showing relevant cross-peaks; NB: indicated labelling of nuclear environments does not correspond to labelling scheme of acetylenic carbons in manuscript.*

** Cross-peak arising from unidentified impurity.*

S2.3 ^{1}H, $^{1}H\{^{31}P\}$, $^{31}P\{^{1}H\}$, and $^{13}C\{^{1}H\}$ NMR spectra of [trans,trans-{Ru(dmpe)$_2$(C≡C^{t}Bu)}$_2$(μ-C≡C-C$_8$H$_{12}$-C≡C)] (3a)

^{1}H NMR (C_6D_6, 400 MHz)
[*trans,trans*-{Ru(dmpe)$_2$(C≡C^{t}Bu)}$_2$(μ-C≡C-C$_8$H$_{12}$-C≡C)] (**3a**)

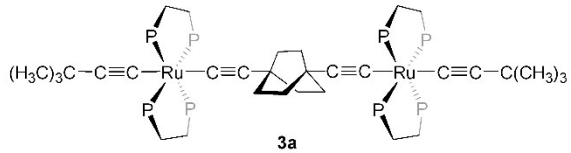

$^{1}H\{^{31}P\}$ NMR (C_6D_6, 400 MHz)
[*trans,trans*-{Ru(dmpe)$_2$(C≡C^{t}Bu)}$_2$(μ-C≡C-C$_8$H$_{12}$-C≡C)] (**3a**)

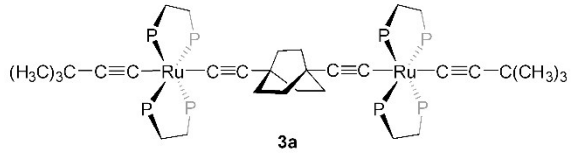

$^{31}P\{^{1}H\}$ NMR (C_6D_6, 162 MHz)
[*trans,trans*-{Ru(dmpe)$_2$(C≡C^{t}Bu)}$_2$(μ-C≡C-C$_8$H$_{12}$-C≡C)] (**3a**)

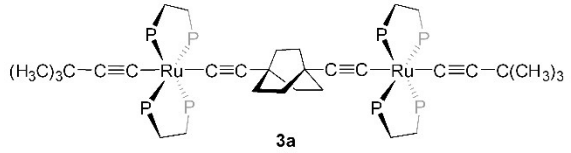

$^{13}C\{^{1}H\}$ NMR (C_4D_8O, 151 MHz)
[*trans,trans*-{Ru(dmpe)$_2$(C≡C^{t}Bu)}$_2$(μ-C≡C-C$_8$H$_{12}$-C≡C)] (**3a**)

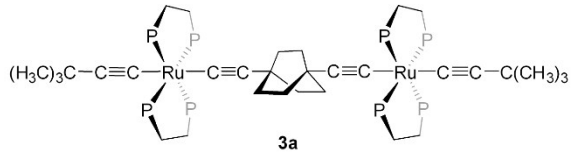

S2.4 ^{1}H, $^{1}H\{^{31}P\}$, $^{31}P\{^{1}H\}$, $^{11}B\{^{1}H\}$, and $^{13}C\{^{1}H\}$ NMR spectra of [trans,trans-{Ru(dmpe)$_2$(C≡C^{t}Bu)}$_2$(μ-C≡C-p-C$_2$B$_{10}$H$_{10}$-C≡C)] (3b)

^{1}H NMR (C_6D_6, 600 MHz)
[*trans,trans*-{Ru(dmpe)$_2$(C≡C^{t}Bu)}$_2$(μ-C≡C-*p*-$C_2B_{10}H_{10}$-C≡C)] (**3b**)

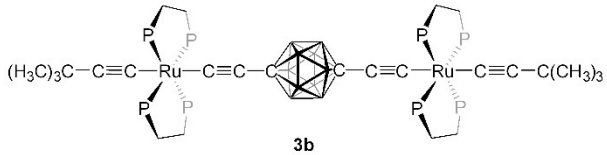

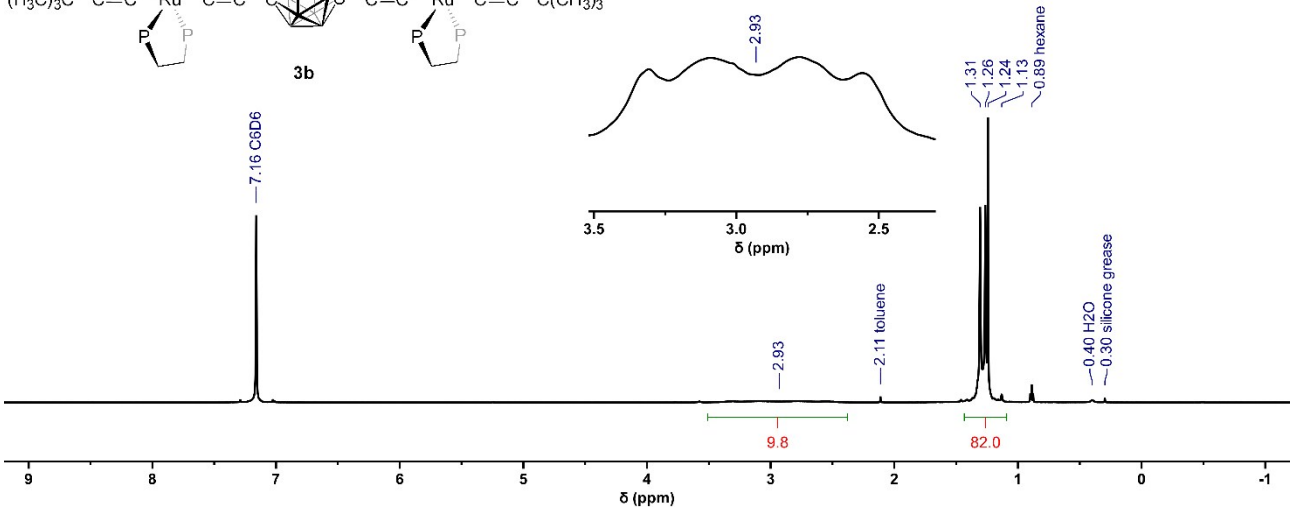

$^{1}H\{^{31}P\}$ NMR (C_6D_6, 600 MHz)
[*trans,trans*-{Ru(dmpe)$_2$(C≡C^{t}Bu)}$_2$(μ-C≡C-*p*-$C_2B_{10}H_{10}$-C≡C)] (**3b**)

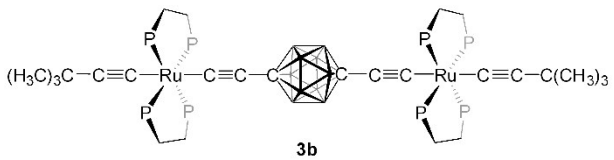

$^{31}P\{^{1}H\}$ NMR (C_6D_6, 243 MHz)

[*trans,trans*-{Ru(dmpe)$_2$(C≡C^{t}Bu)}$_2$(μ-C≡C-*p*-$C_2B_{10}H_{10}$-C≡C)] (**3b**)

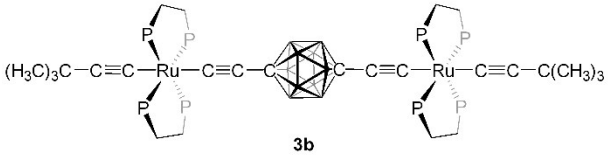

3b

$^{11}B\{^{1}H\}$ NMR (C_6D_6, 193 MHz)

[*trans,trans*-{Ru(dmpe)$_2$(C≡C^{t}Bu)}$_2$(μ-C≡C-*p*-$C_2B_{10}H_{10}$-C≡C)] (**3b**)

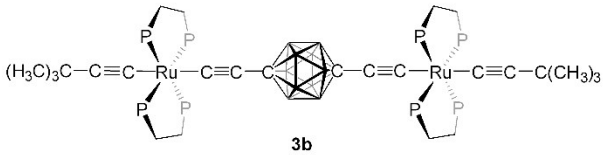

3b

$^{13}C\{^{1}H\}$ NMR (C_6D_6, 151 MHz)

[*trans,trans*-{Ru(dmpe)$_2$(C≡C^{t}Bu)}$_2$(μ-C≡C-*p*-$C_2B_{10}H_{10}$-C≡C)] (**3b**)

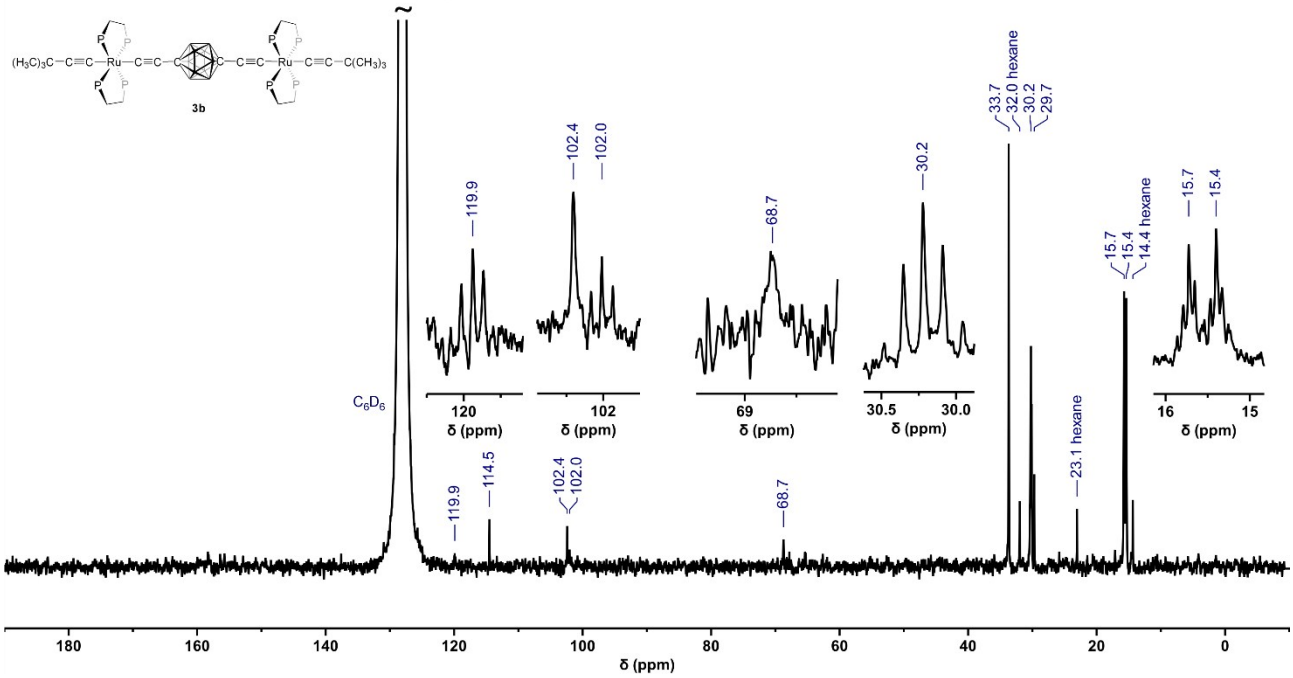

S3 Crystallographic Data

Crystallographic analyses were performed at the Mark Wainwright Analytical Centre at the University of New South Wales.

Data was collected using a Bruker Kappa APEXII area detector diffractometer employing graphite-monochromated Mo Kα radiation generated from a fine-focus sealed tube. The data integration and reduction were undertaken with APEX21, and subsequent computations were carried out with Olex2.

Structures were solved by direct methods with SHELXS and the full-matrix least-squares refinements performed using SHELXL. The non-hydrogen atoms in the asymmetrical units were modelled with anisotropic displacement parameters. Hydrogen atoms were placed in calculated positions and refined using a riding model. All calculations were performed using the crystallographic and structural refinement data summarised in Table S3.1.

For compound **2a**, the six B-level alerts given by the checkCIF report arise due to mild rotational positional disorder of the terminal methyl group attached at C3, and the positional disorder of the two carbon backbone of the dmpe ligands which are known to occupy a number of equivalent bent positions in order to alleviate the steric strain around the ruthenium centre. Parting the atoms in question does not markedly improve the model, thus the model used has elongated ellipsoids indicative of the mild disorder.

Table S3.1 Crystallographic data for [trans-Ru(dmpe)$_2$(C≡C^{t}Bu)(C≡C-C$_8$H$_{12}$-C≡CH)] (2a) and [trans,trans-{Ru(dmpe)$_2$(C≡C^{t}Bu)}$_2$(μ-C≡C-p-C$_2$B$_{10}$H$_{10}$-C≡C)] (3b)

Compound number	**2a**	**3b**
CCDC	1961817	1961818
Empirical formula	$C_{31}H_{51}P_4Ru$	$C_{42}H_{92}B_{10}P_8Ru_2$
Formula weight	648.66	1155.15
Temperature/K	150(2)	150(2)
Crystal system	triclinic	triclinic
Space group	P-1	P-1
a /Å	9.471(3)	9.0326(8)
b /Å	9.9463(13)	9.5696(7)
c /Å	18.892(4)	17.8617(18)
α /°	89.006(15)	80.212(3)
β /°	89.266(19)	87.485(4)
γ /°	79.674(15)	76.091(4)
Unit cell volume /Å^3	1750.4(6)	1476.8(2)
Formula units per cell, *Z*	2	1
ρ_{calc} /g cm^{-3}	1.231	1.299
μ /mm^{-1}	0.648	0.756
F(000)	682.0	602.0
Crystal size /mm^3	0.17 × 0.16 × 0.05	0.18 × 0.1 × 0.05
Radiation	Mo Kα (λ = 0.71073)	Mo Kα (λ = 0.71073)
2Θ range for data collection / °	2.156 to 53.102	4.662 to 50.32
Index ranges	-11 ≤ h ≤ 11, -12 ≤ k ≤ 12, -23 ≤ l ≤ 23	-10 ≤ h ≤ 10, -11 ≤ k ≤ 11, -21 ≤ l ≤ 21
Reflections collected	125061	14559
Independent reflections	7217 [R_{int} = 0.0710, R_{sigma} = 0.0253]	5261 [R_{int} = 0.1171, R_{sigma} = 0.1187]
Data/restraints/parameters	7217/0/327	5261/0/291
Goodness-of-fit on F^2	1.181	1.006
Final R indexes [I>=2σ (I)]	R_1 = 0.0550, wR_2 = 0.1333	R_1 = 0.0577, wR_2 = 0.1393
Final R indexes [all data]	R_1 = 0.0733, wR_2 = 0.1504	R_1 = 0.0896, wR_2 = 0.1589
Largest diff. peak/hole / e Å^{-3}	1.09/-0.69	0.93/-1.11

S3.1 ORTEP Plot of [trans-Ru(dmpe)$_2$(C≡C^{t}Bu)(C≡C-C$_8$H$_{12}$-C≡CH)] (2a)

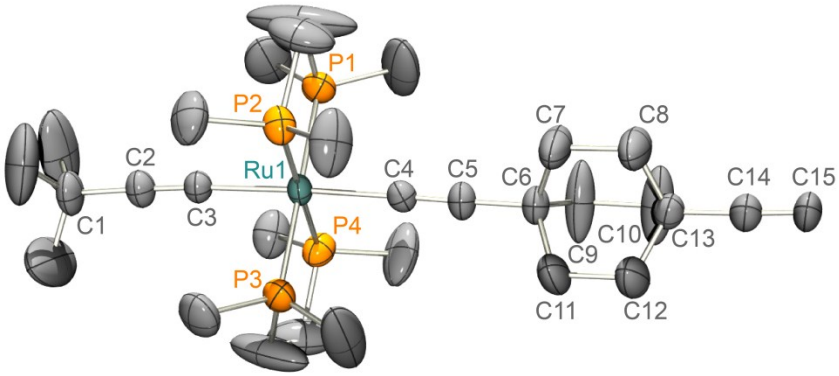

S3.2 ORTEP Plot of [trans,trans-{Ru(dmpe)$_2$(C≡C^{t}Bu)}$_2$(μ-C≡C-p-C$_2$B$_{10}$H$_{10}$-C≡C)] (3b)

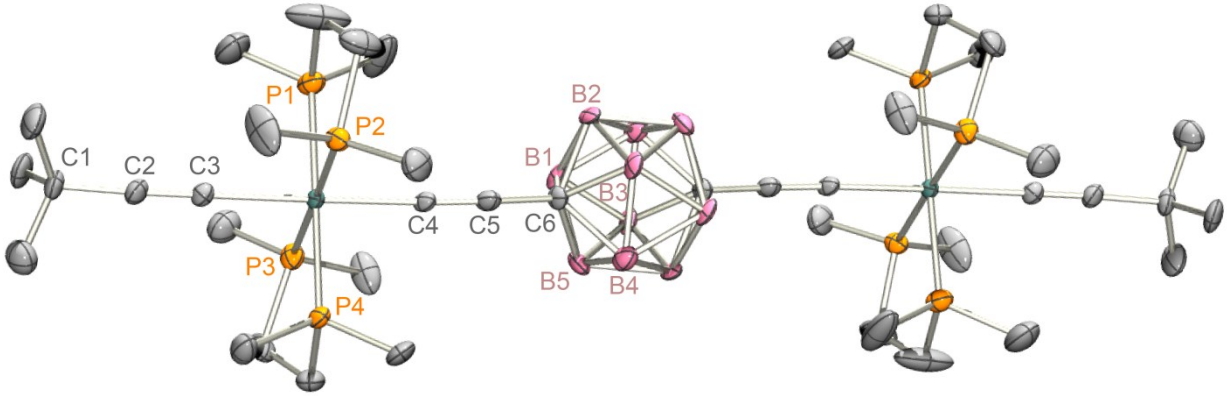

S4 High-resolution Mass Spectra

S4.1 Zoomed mass spectrum of [trans-Ru(dmpe)$_2$(C≡C^{t}Bu)(C≡C-C$_8$H$_{12}$-C≡CH)] (2a)

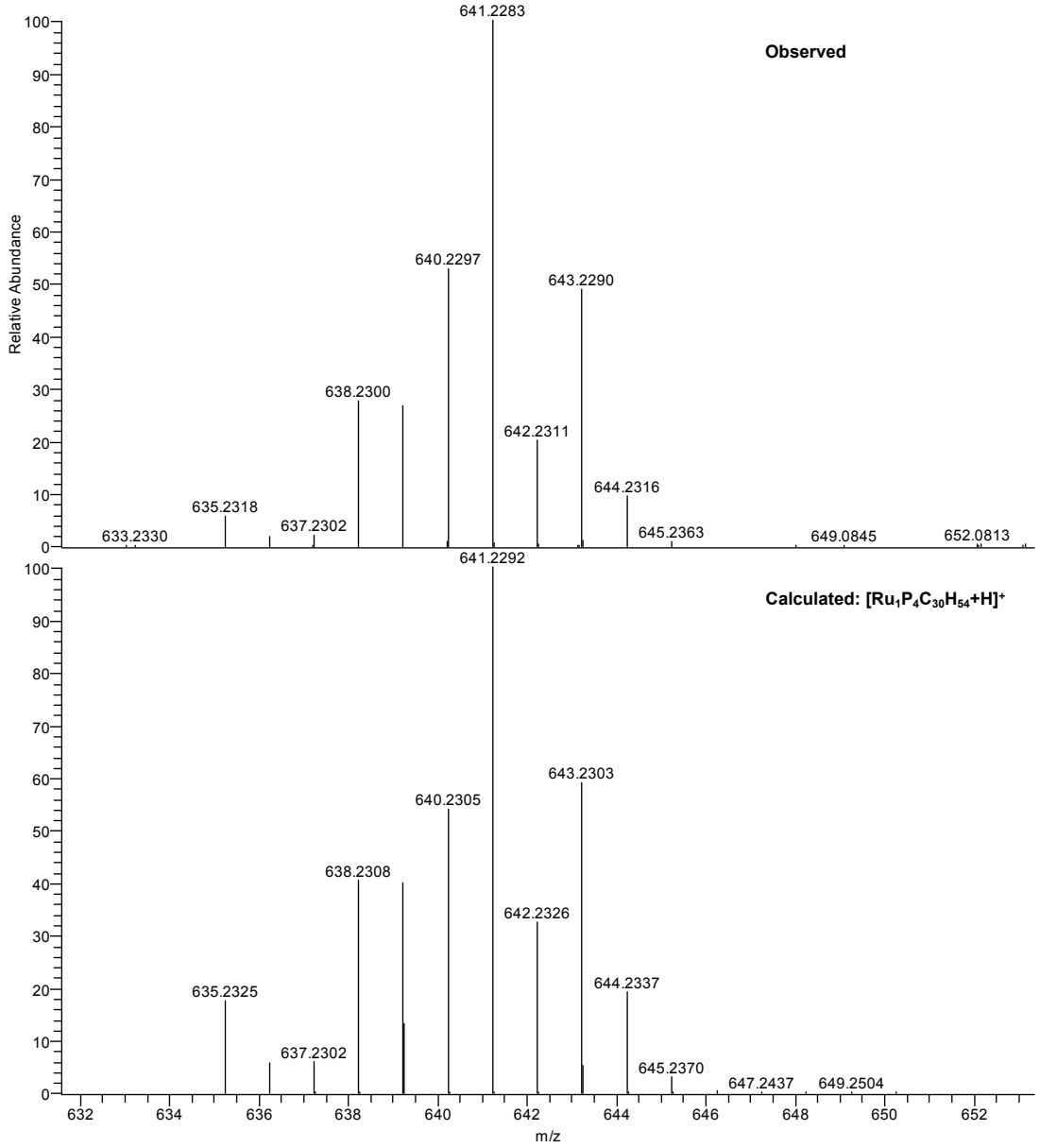

S4.2 Zoomed mass spectrum of [trans-Ru(dmpe)$_2$(C≡C^{t}Bu)(C≡C-p-C$_2$B$_{10}$H$_{10}$-C≡CH)] (2b)

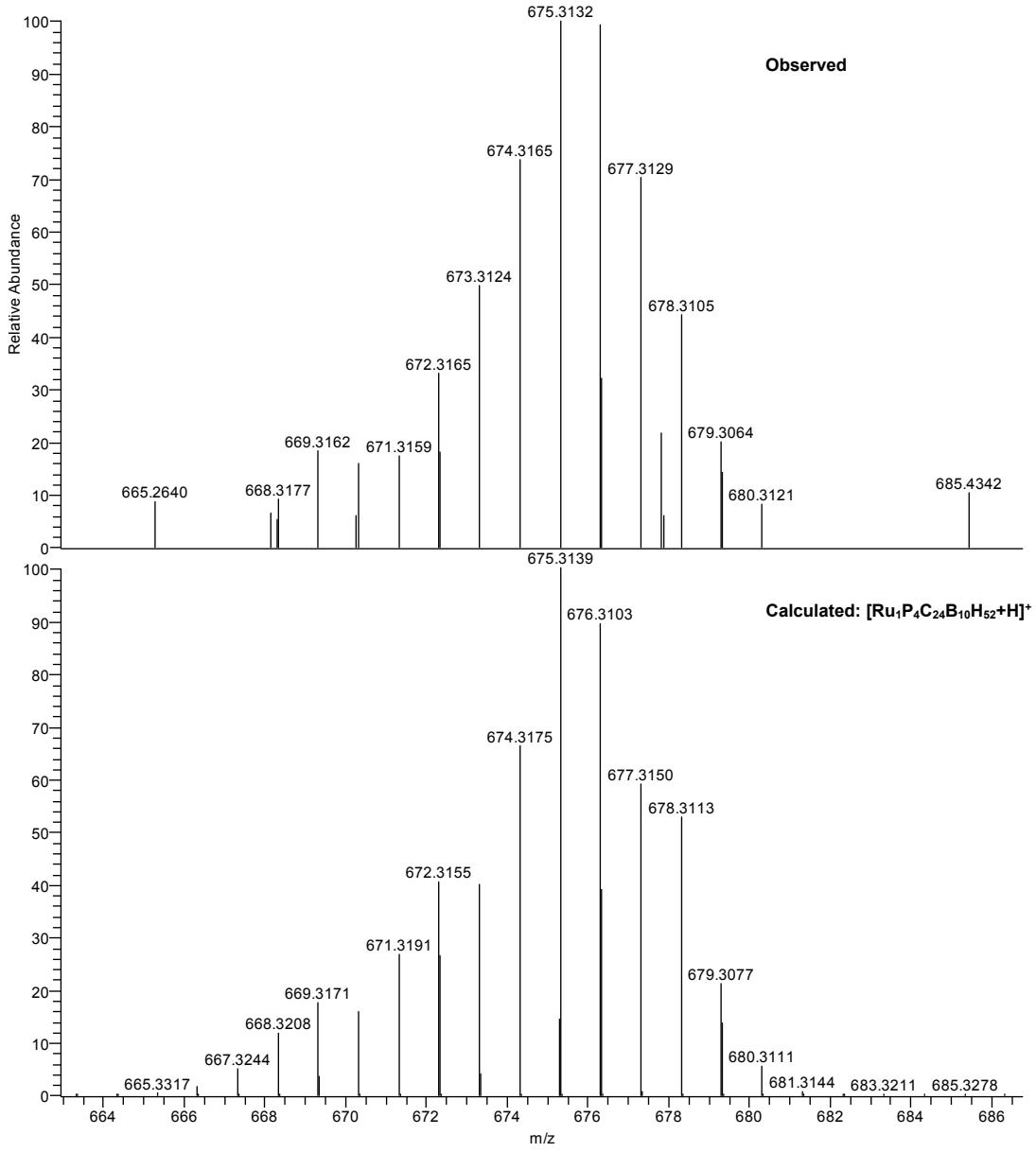

S4.3 Zoomed mass spectrum of [trans,trans-{Ru(dmpe)$_2$(C≡C^{t}Bu)}$_2$(μ-C≡C-C$_8$H$_{12}$-C≡C)] (3a)

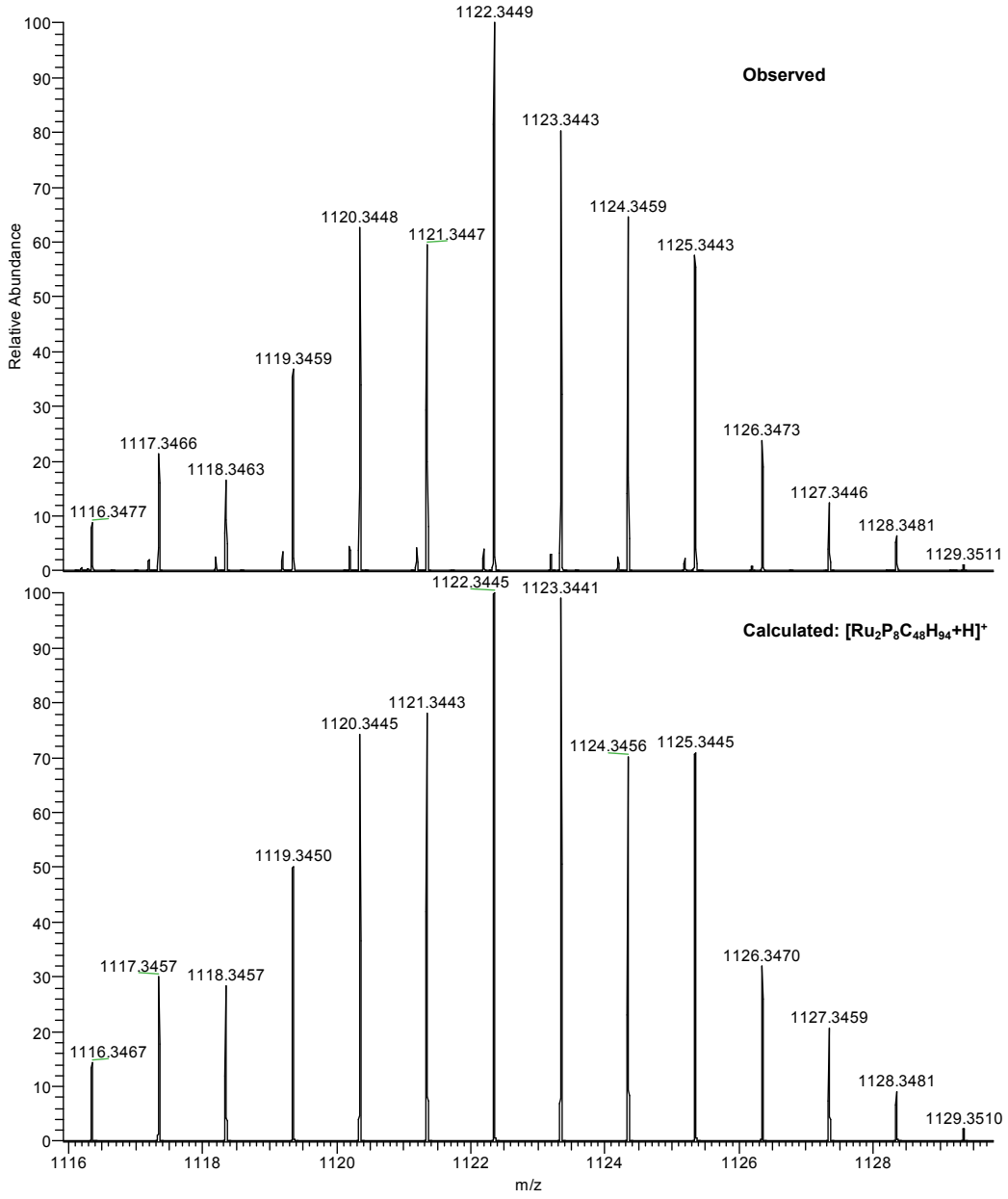

S4.4 Zoomed mass spectrum of [trans,trans-{Ru(dmpe)$_2$(C≡C^{t}Bu)}$_2$(μ-C≡C-p-C$_2$B$_{10}$H$_{10}$-C≡C)] (3b)

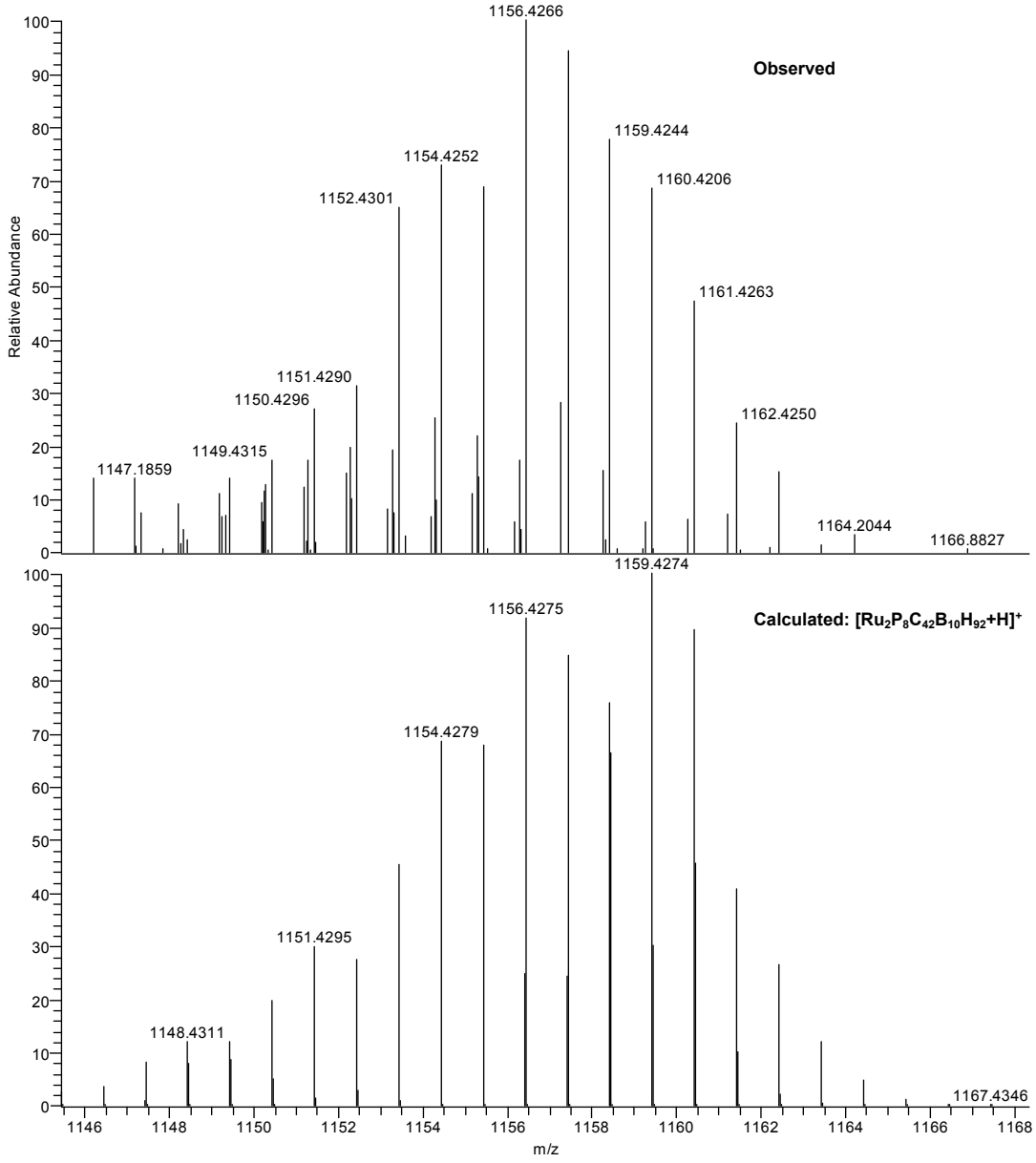

S5 Modelling of Electrochemical Data

S5.1 DPV of [trans,trans-{Ru(dmpe)$_2$(C≡C^{t}Bu)}$_2$(μ-C≡C-p-C$_2$B$_{10}$H$_{10}$-C≡C)] (3b)

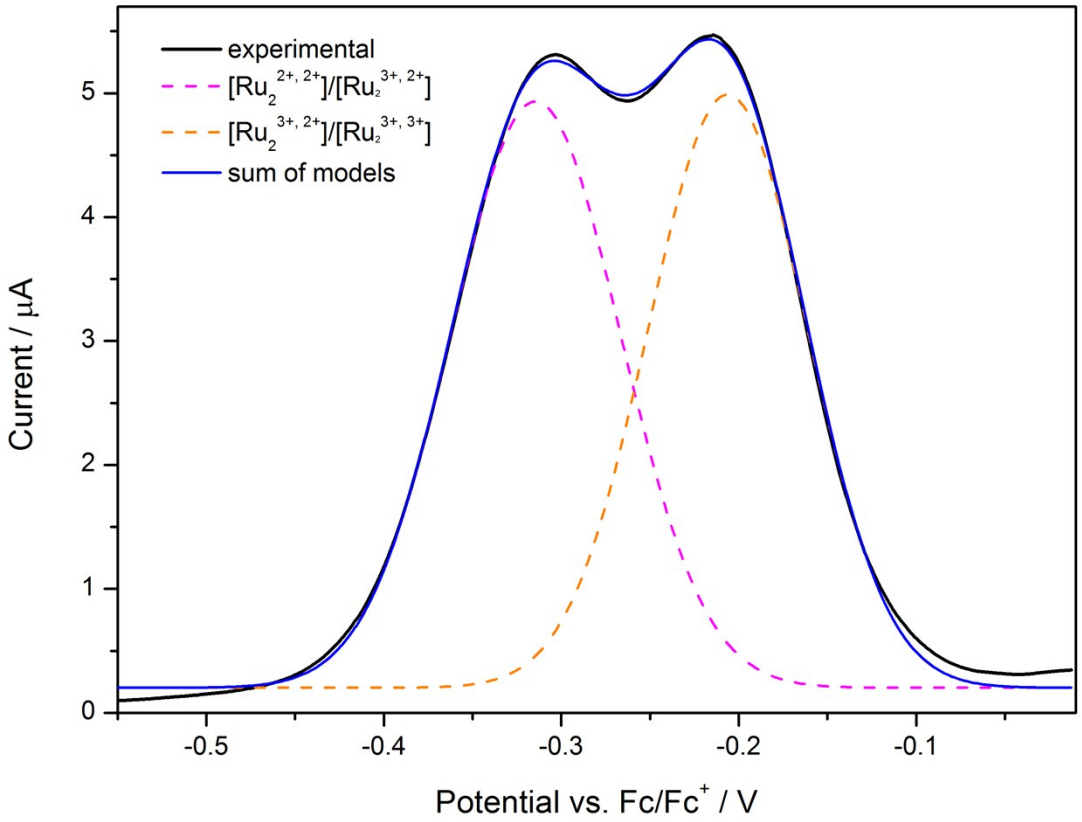

Gaussian deconvolution of DPV performed with Origin Pro 8.1

Table S5.1. Output parameters for peak fitting of DPV of [trans,trans-{Ru(dmpe)$_2$(C≡C^{t}Bu)}$_2$(μ-C≡C-p-C$_2$B$_{10}$H$_{10}$-C≡C)] (3b)

χ^2	0.010	
R^2	0.997	
Peak:	**[Ru$_2^{2+,\,2+}$]/[Ru$_2^{3+,\,2+}$]**	**[Ru$_2^{3+,\,2+}$]/[Ru$_2^{3+,\,3+}$]**
Model	Gaussian	Gaussian
Integration / %	51	49
Peak centre / V	-0.32	-0.21

S5.2 CV simulation of [trans,trans-{Ru(dmpe)$_2$(C≡C^{t}Bu)}$_2$(μ-C≡C-C$_8$H$_{12}$-C≡C)] (3a)

Cyclic Voltammetry (CV) Simulator available at: https://communities.acs.org/docs/DOC-58017-cyclic-voltammetry-cv-simulator-written-in-microsoft-excel[1-3]

A background trace was not subtracted in this simulation.

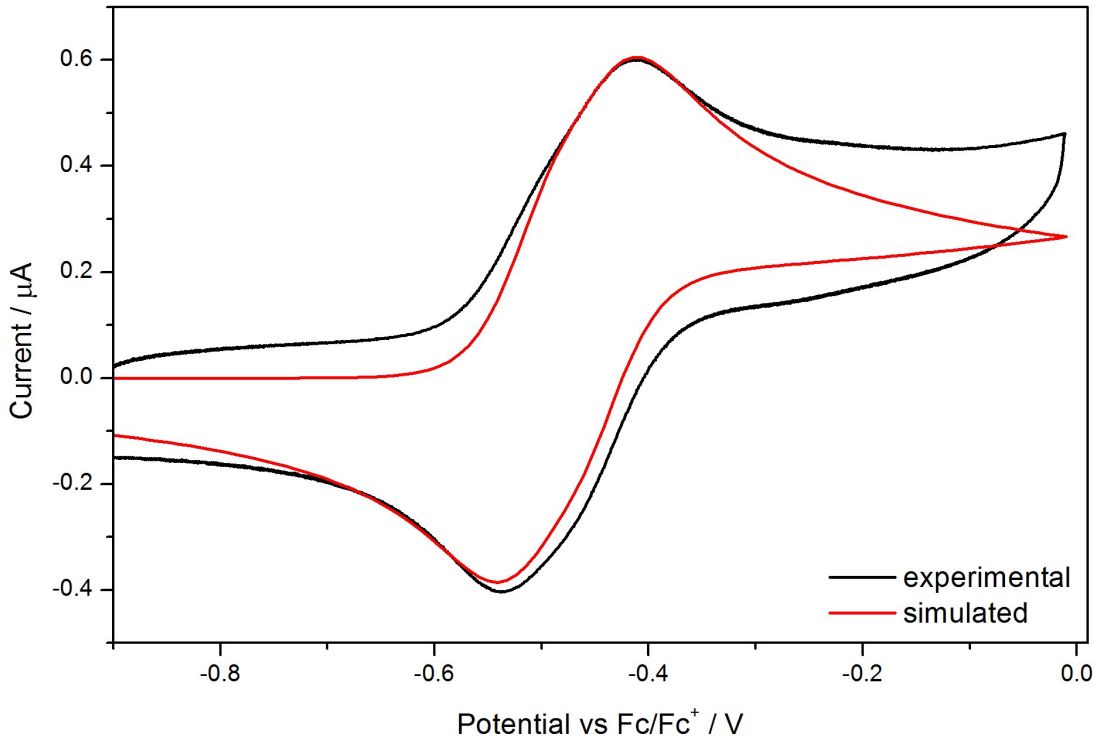

Table S5.2. CV simulation parameters for [trans,trans-{Ru(dmpe)$_2$(C≡C^{t}Bu)}$_2$(μ-C≡C-C$_8$H$_{12}$-C≡C)] (3a)

Bulk concentration / mol cm^{-3}	2.2 × 10^{-7}	
Scan rate / mV s^{-1}	100	
Error (RMS) / □A	7.1 × 10^{-2}	
Redox couple:	**[Ru$_2^{2+,\,2+}$]/[Ru$_2^{3+,\,2+}$]**	**[Ru$_2^{3+,\,2+}$]/[Ru$_2^{3+,\,3+}$]**
$E_{1/2}$ / V	-0.51	-0.44
No. of electrons	1	1
Diffusion coefficient / cm^2 s^{-1}	8.0× 10^{-7}	1.0× 10^{-9}

References:

1. J. H. Brown, *J. Chem. Educ.*, **2016**, *93* (7), 1326–1329. **DOI:** 10.1021/acs.jchemed.6b00052.

2. A. J. Bard, L. R. Faulkner, *Electrochemical Methods: Fundamentals and Applications*, Wiley: New York, **1980**, ISBN: 0-471-05542-5.

3. D. Britz, *Digital Simulation in Electrochemistry 3^{ed} ed.*, Springer: Berlin, **2010**, ISBN: 978-3-642-06307-7.